Focal plane wavefront sensor sensitivity for ELT planet finder

P. Baudoz[a,b], M. Mas[a,b], R. Galicher[c], G. Rousset[a,b]

[a] LESIA, Observatoire de Paris, CNRS, UPMC, Université Paris Diderot; 5 Place Jules Janssen, 92190 Meudon, France

[b] Groupement d'Intérêt Scientifique PHASE (Partenariat Haute résolution Angulaire Sol Espace) between ONERA, Observatoire de Paris, CNRS and Université Paris Diderot.

[c] LUTH, Observatoire de Paris; 5 Place Jules Janssen, 92190 Meudon, France

ABSTRACT

In the framework of Extremely Large Telescope (ELT), several instruments are considered for the characterization of extrasolar planets. Since the performance of such an instrument is limited by wavefront errors, the use of extreme Adaptive Optic (AO) systems is mandatory. Studies for future planet finder instruments such as SPHERE/VLT or GPI/GEMINI show that one limitation of the performance for a planet finder is the differential aberrations that are not measured by the wavefront sensor, which is physically separated from the common optics by a beam splitter. These defects create a field of residual speckles in the focal plane that need to be calibrated to separate the planet signal from the speckle noise [1].

We propose here to simultaneously estimate these aberrations and also detect the planet directly from the final science image. To do so, we propose to couple the foreseen extreme high speed AO of an ELT planet Finder with a low speed Self-Coherent Camera (SCC [2-5]). The SCC which is based on the principle of light coherence can both estimate the wavefront errors and reduce speckle noise by calibration. After recalling the principle of the SCC, we present simulation results of the SCC performance in the context of EPICS.

Keywords: High Contrast Imaging, Coronagraphy, Extremely Large Telescope, Wavefront sensor

1. INTRODUCTION

Exoplanets are typically 10^7 to 10^{10} fainter than their host and are often located within a fraction of an arcsecond from their star. Numerous coronagraphs have been proposed to reduce the overwhelming light of a star to obtain a direct image of its planet [6-9]. But performance is limited by wavefront errors in the upstream beam for all these coronagraphs and stellar speckles dominate the final focal plane image. The effect of most of these aberrations can be corrected by adaptive optics (AO) or eXtreme AO (XAO [10]) but the uncorrected part generates quasi-static speckles, which limit the detection sensitivity [11]. Differential imaging techniques can be used to estimate and reduce this speckle noise. Several solutions exist based on spectral characteristics [12], polarization states [13], differential rotation in image [14], or incoherence between stellar and companion lights [15]. But as shown in Cavarroc et al. [1], any small difference between the images that are compared in these techniques limits strongly their efficiency. The more appealing solution, before using one of these data processing techniques, is to actively suppress quasi-static wavefront errors so that a first speckle reduction is achieved and differential imaging techniques have less work to do. Because of the low level of aberrations that must be achieved (a few nanometers), the best solution is to measure for phase and amplitude errors directly in the final science image to avoid differential errors introduced by classical wavefront sensor. One solution is to directly study the speckle field in the focal plane to retrieve the phase defects upstream of the coronagraph. However, recording image in the focal plane gives only the amplitude of the speckles but not their phase. Solutions exist to measure this phase by introducing known phase in the image [16,17]. However, this requires to record at least two images at different moment and/or with a degraded quality. We propose here to use interference fringes in the focal plane to record the speckle phase in a single coronagraphic image. The instrument we propose, the Self Coherent Camera (SCC), creates Fizeau interferences in the coronagraphic image that can be used to measure complex amplitude in the

Adaptive Optics Systems II, edited by Brent L. Ellerbroek, Michael Hart, Norbert Hubin, Peter L. Wizinowich,
Proc. of SPIE Vol. 7736, 77365S · © 2010 SPIE · CCC code: 0277-786X/10/$18 · doi: 10.1117/12.858272

focal plane but can also be used in a second time as a differential imaging system based on incoherence between speckle light and planet light. The principle and the capabilities of the Self Coherent Camera have already been described [2-5] but mostly in the context of space-based observations. In this paper, we study the capability of the SCC as a ground based instrument to measure the static aberrations after an extreme AO system on a ground-based telescope. We also study the planet detection performance of the SCC coupled with the Spectral Differential Imaging (SDI) technique. The simulations are made in the framework of the planet finder of the European Extremely Large Telescope (E-ELT), which is called EPICS [18].

2. PRINCIPLE

The self-coherent camera (SCC) use spatial interferences in the science image to encode the stellar speckles which are directly linked to the wavefront aberrations upstream of the coronagraph. This section briefly recalls the principle of the self-coherent camera (SCC), which can :

1) measures the uncorrected residual phase directly from the final science image

2) extracts the image of a planet from the residual speckles.

The Figure 1 (left) presents a principle sketch of the SCC. A deformable mirror, located in a plane conjugated to the entrance pupil, reflects the beam incoming from the telescope. We then split the beam. In one channel, the beam goes through a coronagraph. In the other channel, we suppress all the companion light with a spatial filter and extract a beam containing only light from the hosting star. Finally, we recombine the two beams in a Fizeau scheme to obtain spatial fringes in the science image on the detector. Phase and amplitude aberrations give residual speckles in the last focal plane. Since no companion light is transmitted through the second channel, spatial interferences will only affect stellar speckles whereas it does not have any impact on a possible planet image since companion light is not coherent with star light. The stellar speckles are thus spatially encoded (modulated) whereas the planet image is not.

The mean intensity of residual speckles of the coronagraphic channel is relatively flat over a field of view of diameter of a few tens of λ/D and it is also very attenuated because of the coronagraph (see Figure 2, left for example). To optimize fringe contrast, we match intensity distributions and fluxes of both channels. To do so, we decrease the diameter of the diaphragm of the spatially filtered channel (D_R) compared to diameter of the coronagraphic pupil (D) in order to obtain an almost flat intensity in the focal plane ($D>>D_R$). We can notice that this diaphragm reduces the impact of aberrations on this reference channel since only a few λ/D_R are visible in the image. Thus, this channel is not very sensitive to aberrations and can be calibrated before the interference recording [5]. Fluxes can also be equalized using a variable neutral density or by condensing the light in the reference channel before the pinhole.

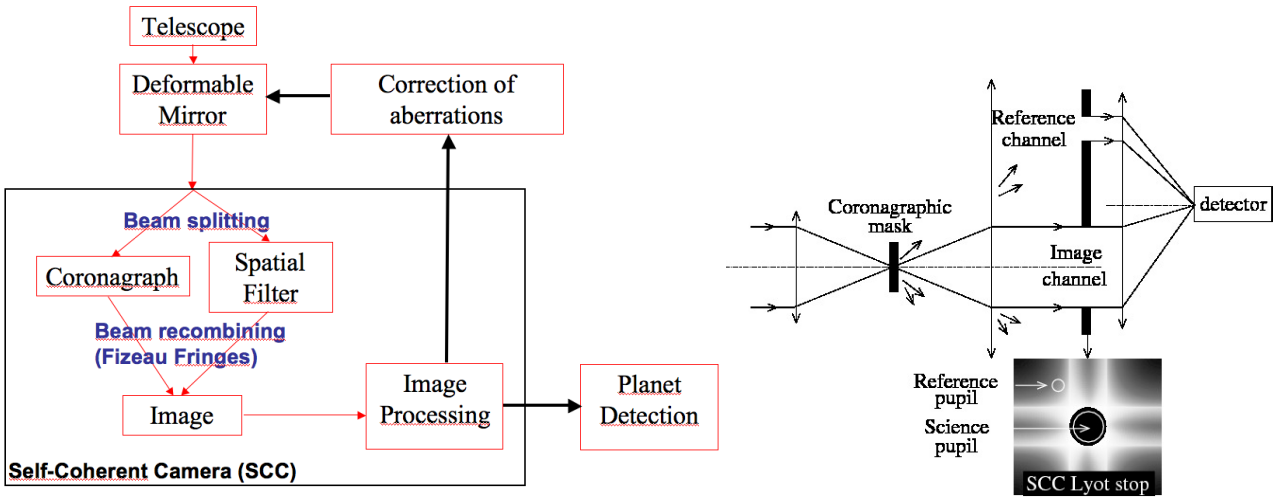

Figure 1: *Left:* General principle of the Self-Coherent Camera. *Right:* Example of a possible optical design of SCC with a coronagraph which uses a Lyot stop. An additional hole in the classical Lyot stop creates the SCC reference channel. The light distribution in the Lyot stop is shown for the case of the Four Quadrant Phase Mask coronagraph [7].

Several optical set-ups have been proposed based on classical interferometry or exploiting diffraction characteristic of focal mask coronagraphs [5]. The last solution is very appealing since it couples the four elements of the SCC (beamsplitter, coronagraph, spatial filter, Fizeau recombination) in two simple elements: a focal mask coronagraph and a Lyot stop modified with a small hole located at a few D from the optical axis (Figure 1, right). This solution also removes the need for a delay line and the possible variation of the optical path difference that comes with it. In Figure 2 (left), we present, at the same spatial scale and for an instantaneous snapshot after an extreme adaptive optic system used on the E-ELT, an image after the coronagraph which shows residual speckles, an image corresponding to the reference channel for a pupil of diameter D_R=D/85 and an interferential image where the residual speckles are spatially encoded by fringes.

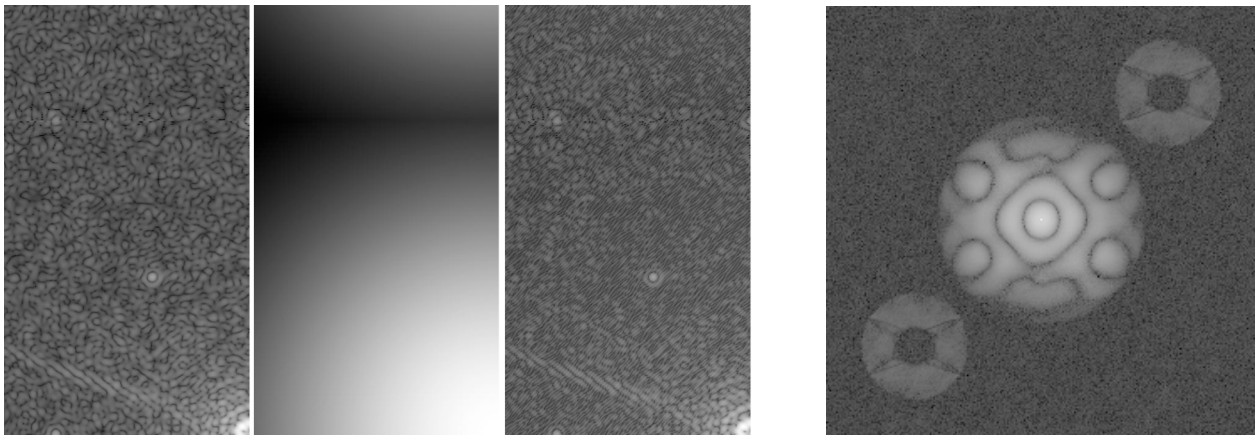

Figure 2. *Left:* This figure shows 3 times the same part of the simulated detector for different cases: (a) Image formed after the sole coronagraph. (b) Image of the sole reference channel. (c) Interferential image where the speckles are spatially encoded by fringes. The scale is the same for (a) and (c) and has been enhanced for (b) to better see the intensity distribution of this channel. Only part of the detector is shown. Center of all images (corresponding to coronagraph axis) is located on the lower right side. Diffraction effects from E-ELT spider arms and holes between segments are visible in images (a) and (c). Monochromatic images. *Right:* Fourier transform of SCC image (c) which shows three correlation peaks.

Below, we develop a simplified monochromatic formalism to describe the propagation of light and the data processing for the SCC.

Assuming a perfect coronagraph [1], we can describe light distribution in the modified Lyot stop as:

$$\left(P_S(\xi).\exp(i\phi(\xi)) - \alpha.P_S(\xi)\right) + P_R(\xi) * (\xi - \xi_0) + P_P(\xi) \qquad \text{Eq. 1}$$

The first term describes the perfect coronagraph which removes a weighted perfect pupil to the aberrated pupil. The coefficient α minimizes the subtraction of the coherent core of the point spread function. It is in fact equal to the instantaneous value of $S_r^{1/2}$, S_r being the coherent energy (or Strehl ratio): $S_r=\exp(-\sigma_\phi^2)$ with σ_ϕ^2 the spatial variance of the phase ϕ.

P_S, P_R and P_P describe the pupil shape and amplitude for respectively the star, the reference channel, and the planet. Both P_S and P_P have a diameter D corresponding to the Lyot stop diameter while P_R is smaller (diameter D_R << D). ξ is the coordinate in the pupil plane (ξ is a vector).

In the next focal plane, the complex amplitude can be written:

$$A_S(x) + A_R(x).\exp(\frac{i2\pi.x.\xi_0}{\lambda}) + A_P(x) \qquad \text{Eq. 2}$$

A_S describes the complex amplitude in the focal plane when a coronagraph is used:

$$A_s(x) = TF\left[P_S(\xi).\exp(i\phi) - \alpha.P_S(\xi)\right] \quad \text{Eq. 3}$$

with TF(u)=û describing the Fourier transform, which is a simplification of the optical propagation from pupil plane to focal plane.

From Eq 2., we can derive the intensity in the focal plane:

$$I = I_S(x) + I_R(x) + I_P(x) + \mathrm{Re}\left(A_S(x)A_R(x)^*\right).\cos\left(\frac{i.2\pi.x\xi_0}{\lambda}\right) \quad \text{Eq. 4}$$

With $I_i=|A_i|^2$. Fringes only appear on the stellar residuals because the planet light is not coherent with the stellar flux.

I is the image that is recorded in the focal plane of the SCC. From this image, we start the SCC data processing by applying a Fourier transform to the image:

$$\hat{I} = \hat{I}_S + \hat{I}_R + \hat{I}_P + \left[\left(P_S.\exp(i\phi) - \alpha.P_S\right).P_R^*\right] * \delta(\xi + \xi_0) + \left[\left(P_S.\exp(i\phi) - \alpha.P_S\right)^*.P_R\right] * \delta(\xi - \xi_0) \quad \text{Eq. 5}$$

If ξ_0 is large enough, we obtain three separated peaks in the UV plane Î (see Figure 2, right) and we can rewrite Eq. 5:

$$\hat{I} = \hat{I}_C + \hat{I}_- * \delta(\xi + \xi_0) + \hat{I}_+ * \delta(\xi - \xi_0) \quad \text{Eq. 6}$$

We can select in the UV plane each peak, center it and apply a Fourier transform to obtain separately the images I_C, I_+, and I_-. The detection of the planet can be done by simply using these images [2]:

$$I_P = I_C - I_R - \frac{I_+ I_-}{I_R} \quad \text{Eq. 7}$$

That is one of the capabilities of the SCC. As described in Section 2, we only see the central core of the reference point spread function. Thus, it should be less sensitive to aberrations and temporal variations. Assuming I_R is stable and that we record an image before the observation, all other parts of Eq. 7 are calculated from the SCC image I. As shown in [2,3], the speckle noise is fully removed in monochromatic light and in that case, planet detection capability is then only limited by photon noise.

As described above, we can also measure the wavefront error. This is done by only using one of the lateral peak, for example I_-:

$$TF\left[\frac{I_-}{A_R^*}\right] = P_S.\exp(i\phi) - \alpha.P_S \quad \text{Eq. 8}$$

In the case of small aberrations, Eq. 8 can be simplified using $\exp(i\phi)\approx 1+\phi$ and $\alpha\approx 1$:

$$TF\left[\frac{I_-}{A_R^*}\right] = P_S i\phi \quad \text{Eq. 9}$$

For small phase defects, there is a linear relation between I_- and the phase aberration upstream of the coronagraph. We need to know the complex amplitude distribution of A_R. Since we are only interested in the core of A_R, which is not very sensitive to aberrations, we can use I_R to estimate A_R or use a model of its light distribution [5].

3. THEORETICAL PERFORMANCE

3.1 SCC as a static aberration wavefront sensor

While the SCC appears as a very promising approach for high precision adaptive optics (AO) on space-based telescope [4], it can certainly not replace a classical AO system on ground-based telescope. Indeed, the computation time needed and more importantly the chromatic limitation [4] of the instrument which requires the use of a Wynne corrector [19] or the use of an integral field spectrometer implies that it is less sensitive than classical AO for fast phase measurements.

Besides, SCC requires about three times more pixels than other wavefront sensor, implying a larger sensitivity to detector read out noise. However, since it is able to measure the aberrations in coronagraphic images and directly from the final images, it appears as a very interesting instrument to estimate precisely the static aberrations, which are strong limitations in high dynamical range imaging.

For ground-based observation, the phase aberrations ϕ is the sum of the turbulent phase ϕ_{turb} and the static errors ϕ_{stat} :

$\phi = \phi_{turb} + \phi_{stat}$

If the exposure time is longer than the turbulent speckle life time, we can assume there are enough independent realizations to write the temporal mean of Eq. 8 and :

$$\left\langle TF\left[\frac{I_-}{A_R}\right]\right\rangle = P_S.\exp(i\phi_{stat}).\left\langle \exp(i\phi_{turbu})\right\rangle - \langle\alpha\rangle.P_S \qquad \text{Eq. 10}$$

Assuming that spatial variance and temporal variance of the phase are equal $\langle\exp(i\phi)\rangle = \exp(-\sigma_\phi^2/2) = S_r^{1/2} = \alpha$, we can also write, assuming small aberrations:

$$\left\langle TF\left[\frac{I_-}{A_R}\right]\right\rangle = P_S.\exp(i\phi_{stat}).\langle\alpha\rangle - \langle\alpha\rangle.P_S \approx P_S.i\phi_{stat}.\langle\alpha\rangle \qquad \text{Eq. 11}$$

where $\langle\alpha\rangle = S_r^{1/2}$ with S_r the mean Strehl ratio describing the corrected turbulence. Thus, the estimator of the static phase errors equals the one derived in the case of short exposure time [4] divided by a constant number equal to $S_r^{1/2}$.

3.2 Phase measurements

To evaluate the capability of the SCC as a slow wavefront sensor coupled with a fast extreme AO, we numerically simulated an XAO system applied on the E-ELT and introduced small static aberrations. The simulation assumes an unobstructed E-ELT equipped with a deformable mirror made of 210x210 actuators and a Self-Coherent Camera. The Self Coherent Camera is simulated with a perfect coronagraph. The spatially filtered channel is assumed to be perfect with a diaphragm size D_R=D/85. No detector noise is taken into account. The turbulent residual after XAO correction of 64 nm RMS is derived from the Power Spectral Density (PSD) of the extreme adaptive optics calculated by the EPICS team [10]. For this first simulation, the evolution of turbulence is simulated by using independent wavefront maps that are supposed to last the lifetime of the coherent time (here 10 ms at the working wavelength bandwidth R : λ_0=700 μm, $\Delta\lambda$=0.22 μm). The static aberration PSD evolves as f^{-2} where f is the spatial frequency.

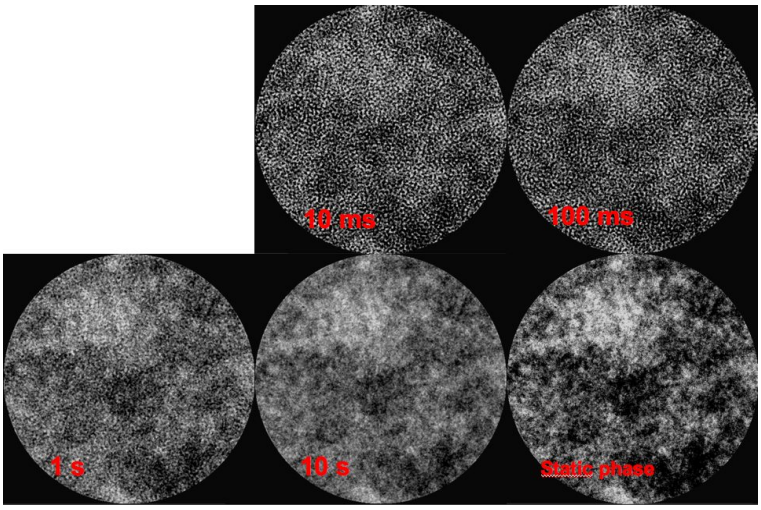

Figure 3. Reconstructed phase via the Self-Coherent Camera for different exposure times. Assuming a coherent time of 10 ms, static aberration of 1 nm, and amplitude of the residual turbulent phase inside DM frequency :40 nm

To be able to estimate the static phase, it is necessary to average out the turbulent phase (Figure 3). The precision we can reach on the estimation of the static phase ($\sigma_{\Phi stat}$) is then directly related to the turbulent phase residual level ($\sigma_{\Phi turbu}$) and to the number of independent turbulent realizations (Nb_indpt) that has been reached :

$\sigma_{\Phi stat} = \sigma_{\Phi turbu} / \mathrm{sqrt}(\mathrm{Nb\_indpt})$

Roughly, for a residual turbulent phase of 40 nm inside the spatial frequency that can be corrected by the XAO (64 nm total), to reach a precision of 1 nm, it requires more than 1600 independent realizations. Assuming a 10 ms coherent time, analytically it would need 20 s to reach a 1 nm precision. The simulation shows that this is the approximate time needed. In Figure 4, we estimate the time necessary to measure the static aberration to 1 and 0.3 nm RMS for a given star magnitude with the SCC. For very bright stars (magnitude R<6), this time is only limited by the averaging of residual turbulent aberrations. As expected, we found that this residual noise on the phase estimation is linearly proportional to the amplitude of turbulent residual aberrations after XAO and inversely proportional to the square root of the number of independent turbulent simulated phase screens. For fainter stars, photon noise dominates the noise from the averaging of residual turbulent aberrations. The results are very promising since it appears that we can reach a low level of optical defects (1 nm RMS) in a relatively short time (a few tens of seconds) for the expected average magnitude target. As reported in Cavarroc et al. [1], the theoretical level of residual speckle varies as the inverse of the square of the RMS amplitude of these aberrations. So decreasing this level to 1 nm RMS brings a gain of 400 compared to an hypothesis of 20 nm RMS [1].

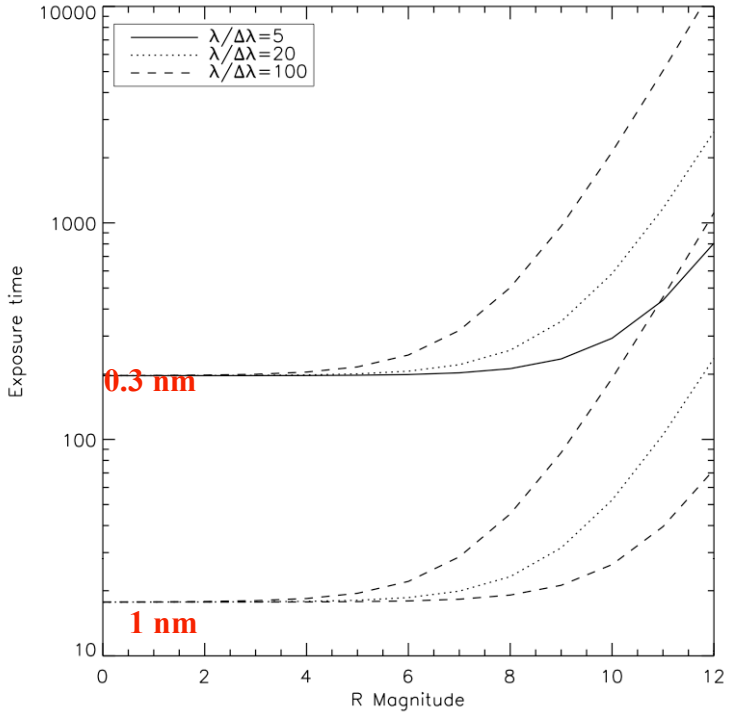

Figure 4. Exposure necessary to measure static aberration with levels of 1 nm and 0.3 nm as a function of magnitude. Curves show several spectral resolutions. The bandwidth is centred on R band. Turbulence PSD takes into account 210x210 actuators (64 nm residual). Coherent time :10 ms. The level of residual aberrations is measured in the central 90 % of the corrected area. Simulation takes into account photon noise limitation and phase-averaging limitation.

3.3 Application to quasi static phase aberration measurements

Above, we took the hypothesis that the optical aberrations created in the telescope were fully static. Unfortunately, this is optimistic and we need to study the impact of long or short term variation of these quasi-static aberrations. To do so, a second simulation has been developed. We also changed the way the turbulent phase aberration is simulated. Instead of simulating independent phase screens every 10 ms, we simulate complete turbulent layers and translate them in front of our numerical pupil. For calculation time reason, we did not simulate an E-ELT XAO but instead used the SPHERE/XAO configuration (40x40 actuators over a 8m diameter pupil). The sampling in the pupil plane is 10

cm/pixel. We simulate 2 orthogonal layers with a Fried parameter r_0=1m in the observing wavelength (H band), an outer scale of 20 m, and a wind speed of 10 m/s.

To simulate the AO correction, first, we estimate the phase measured by a wavefront sensor limited to spatial frequencies that the deformable mirror can correct (40x40). This estimation is calculated by a Fourier filtering of the needed spatial frequencies. Then, we apply this correction of the phase but with a temporal delay of 1 ms (it is our sole error in this case). The residual aberration amplitude over the pupil after correction is then approximately of 35 nm RMS. We simulate 100 images per second and integrate these 100 SCC images before calculating the phase estimation by the SCC algorithm. From this 1s image, we estimate the measurement errors for static aberrations and for quasi-static aberrations. The quasi-static aberrations are simulated as a combination of static aberrations so that the phase screen is completely uncorrelated after 20s. The complete simulation data reproduces a 100 s observation. No photon noise is introduced in this simulation.

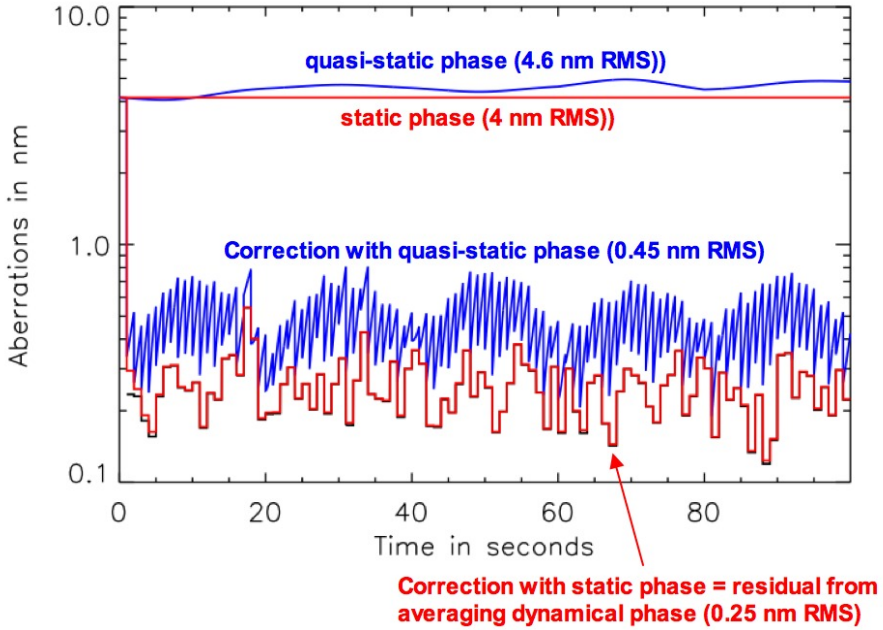

Figure 5 : Amplitude defects (top) and estimation errors (bottom) for static aberrations (dashed line) or quasi-static aberrations (doted line). The amplitude of the defects and the estimation errors are both given in nm RMS. The residual error from averaging of the dynamical turbulent phase is also shown (solid line).

While the estimation errors for static aberrations are limited by the turbulent phase measurement (Figure 5), the quasi-static variation introduces an error for the estimation of the phase. Its level is however relatively low (0.45 nm RMS compared to 0.25 nm RMS for fully static aberrations) for an amplitude of the quasi-static aberrations of 4.6 nm. If the phase errors that need to be corrected have a longer correlation time, it is possible to increase the exposure time used to estimate the aberrations and then improve the SCC phase estimation. The correlation time and amplitude of the quasi-static aberrations are poorly constrained. We expect to get better information on this with SPHERE for the VLT. A good estimation of these values in the case of the E-ELT is also necessary to calculate more precise capability of EPICS.

4. APPLICATION TO EPICS

In this section, we simulate the use of the SCC as a high contrast imaging instrument mode for the planet finder of the European-Extremely Large Telescope (E-ELT). The study is done for the visible wavelength between 0.6 and 0.8 µm, which corresponds to the R band. While Strehl ratio is higher in near IR images allowing better coronagraph performances (coupled with lower star-planet contrast in some cases), we decided to study a SCC in the visible wavelengths because of the technical availability of detector able to freeze the speckles with virtually no readout noise. If such detectors become available in the near IR in the future, this instrument could also be proposed in the near IR. The detection of planets is done using two adjacent narrow filters (R=20), which can be used for spectral differential imaging (SDI) and for photometry analysis. This coupling of SCC and SDI helps to mitigate the limiting effects of both

techniques: chromatic dependency of the fringes for the SCC [4] and differential aberrations sensitivity for SDI [1]. Simulation assumes a field of view relatively small (0.4"x0.4"), which represents about 100x100 λ/D and is quite optimized for planet detection. Indeed, assuming an inner working angle for the coronagraph (i.e., the closest angular distance for planet detection) of 2 λ/D (7 mas), we can scan the distance between 0.07 and 2 AU around a star located at 10 parsecs. We assume typical snapshots of 10 ms for the detector to freeze the residual atmospheric turbulence.

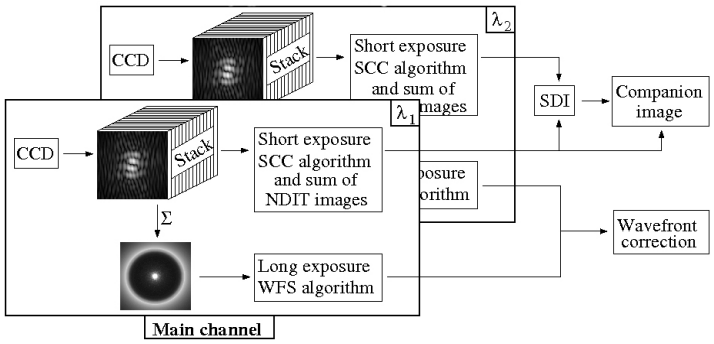

Figure 6: SCC functional diagram and data organization

We simulate the operation of the SCC instrument by calculating 10ms snapshots using hypothesis described in Section 3.2 but using an obstructed E-ELT pupil design. These snapshots are immediately used in two different ways (Figure 6):

- On one side, the snapshot is added to previous snapshots to create a long exposure time image (this is actually a moving average to decrease integration noise). **This long exposure time image is used to estimate the simulated ELT static wavefront errors using properties of the SCC as described in section 2 using Eq. 11.** This information on the phase and amplitude defects of the beam is then used to simulate the correction of theses defects by the EPICS deformable mirror. This first step ensures that the aberration level of residual static wavefront errors is very low. It also helps to correct for amplitude errors of the ELT in one half of the field of view. The left part of the image in Figure 7 is free of the diffraction peaks created by gaps and amplitude variations of the ELT segments. We can however introduce uncorrected aberrations to estimate their impact on the planet detection.

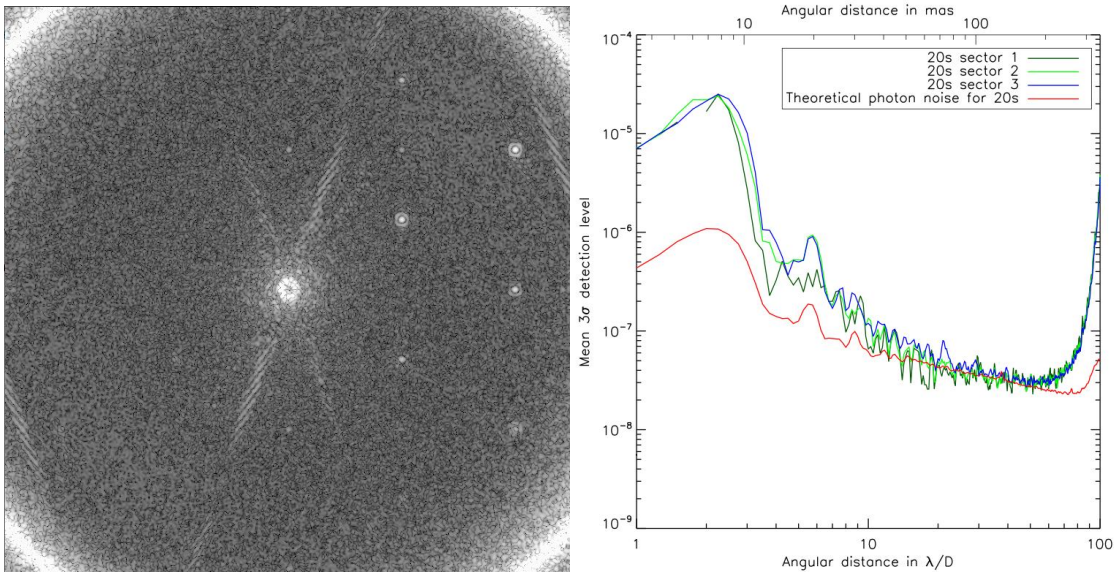

Figure 7 : Left: Subtraction of two polychromatic SCC processed images centred in λ_1 and λ_2. Right : Detectability at 3 σ for different area differential imaging of SCC processed images. Exposure time is 20s and 3 sectors are used to estimate the detectability. Comparison with coronagraphic photon noise level. Spectral bandwidths : λ_1=0.7μm and λ_2=0.735μm and R=λ/Δλ=20 for both. Magnitude 4. RON=1 e-/pixel. No common static aberrations

- On the other side the data are kept for planet detection. **The aberrations potentially not corrected still appear as fringed speckles on the focal plane and a post-processing algorithm based on Eq. 7 is used to perform the ultimate planet detection.** This second step can be compared to the differential techniques described in Sect. 1 using incoherence between the star and the planet to discriminate stellar speckles from a planet. We first apply the SCC processing on each spectral bandwidth, then we subtract one processed image to the other.

The simulation result presented in Figure 7 shows that the detection limit of the SCC coupled with SDI reaches the photon noise limit starting at 3 λ/D. The results is shown for 20s only but it already corresponds to a simulation of 2000 independent chromatic SCC image in each spectral bandwidth.

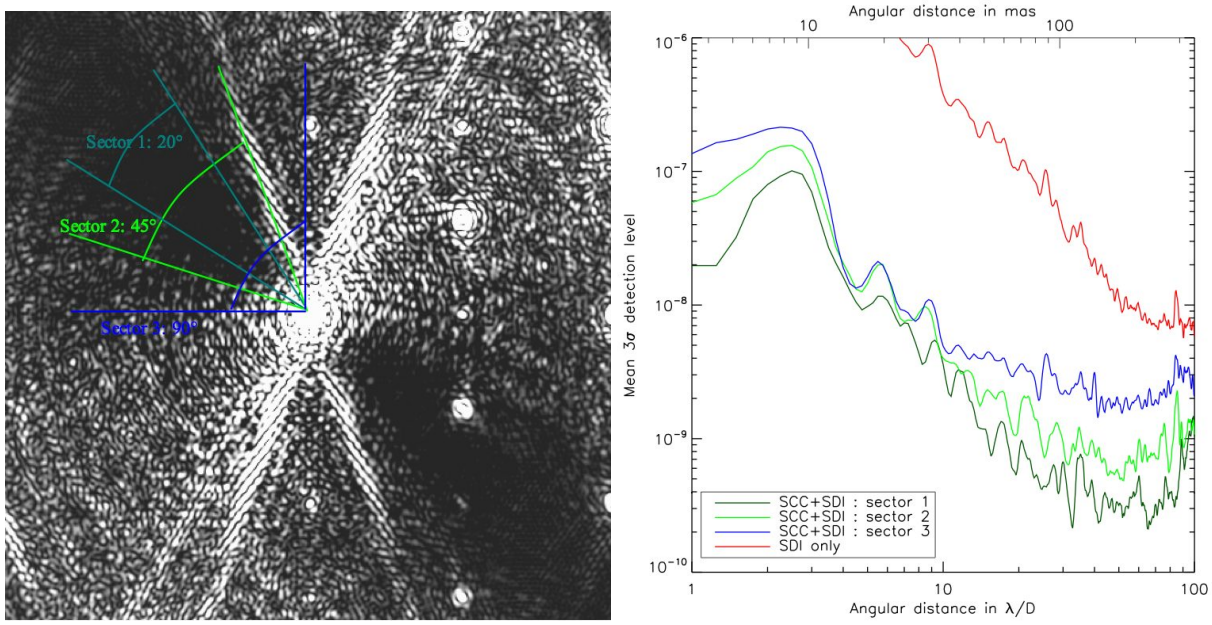

Figure 8 : Left: Subtraction of two polychromatic SCC processed images centred in λ_1 and λ_2. Right : Detectability at 3 σ for differential imaging of SCC processed images as a function of angular distances. Hypothesis for both: differential aberration of 1nm between the two wavelengths. No turbulence, no photon noise. Spectral bandwidths : λ_1=0.7μm and λ_2=0.735μm and R=λ/Δλ=20 for both. Common static aberrations :5 nm

We know that differential aberrations (aberrations which differ between the two chromatic bandwidths) have a strong impact on spectral differential imaging (SDI). We investigate the impact of differential aberrations on our case of differential imaging of SCC processed images. Assuming no atmospheric turbulence, we add differential aberrations between both wavelength paths. The limitation level is found to be 100 times lower than for classical SDI. A 1 nm differential aberration introduces limitation level of roughly 10^{-9} (Figure 8). Obviously, the level reachable varies with area on the detector and we find a better detectability level in the sector where the SCC processing is less sensitive to chromatism, i.e. in the fringe direction. It is important to notice that this is certainly not the lowest level reachable by the instrument since angular rotation of the field of view can also be used in our instrument to improve the detection of planets as it will be done on the SPHERE/VLT instrument. The optional solution of coupling the SCC with an IFS could also be used to decrease this level using spectral deconvolution on SCC processed images. We also studied the impact of static aberration before the SCC and found it negligible whenever these errors are lower than 5 nm. As we demonstrated that SCC could measure in less than a minute static aberrations at the level of 1 nm, it should not be a problem. The performance of an instrument taking full benefit of the SCC needs to be studied in more details.

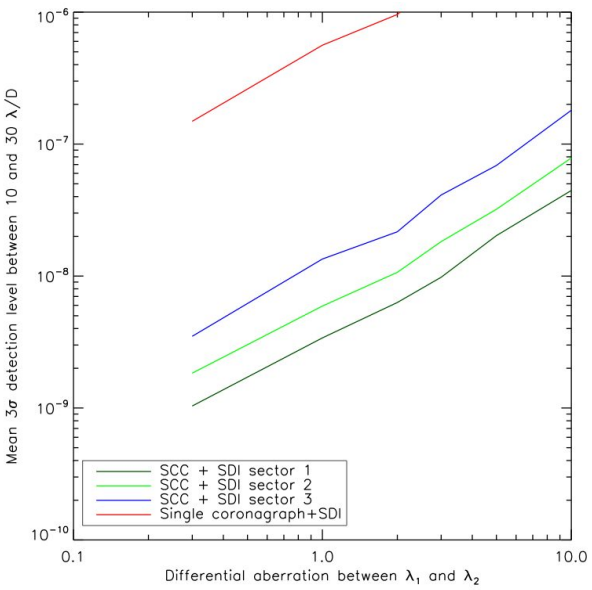

Figure 9 Right: Detectability at 3 σ for differential imaging of SCC processed images as a function of differential aberration and averaged between 10 and 30 λ/D. No turbulence, no photon noise. Common static aberrations :5 nm

5. CONCLUSION

The concept of the Self-Coherent Camera (SCC) is very new and a lot of areas are still to be studied in details. While it has been proposed for space based observation, where it appears to be very promising, use on ground based instrument seems also feasible. It is especially important in the context of EPICS, the planet finder of the E-ELT. Indeed, this ambitious project definitely needs an efficient solution to estimate the static aberrations as well as a powerful instrument for planet detection. The solution proposed by the SCC to perform both is particularly appealing. In this paper, preliminary simulations has been described. It appears that the SCC is able to measure static or quasi-static aberrations efficiently. The level reachable by the SCC depends on several criteria, two of them being poorly constrained: the amplitude and correlation time of quasi-static aberrations. Measurements of these values are needed to estimate more precisely the efficiency of high contrast imaging instrument like the SCC on the E-ELT. Coupled to this phase measurement, SCC also allows us to detect planet in the residual speckles. Preliminary results for an SCC instrument in EPICS have been shown. The SCC data are recorded in two spectral bandwidths that are used to perform Spectral Differential Imaging (SDI). The simulation shows clearly that combination of both techniques is 100 times more efficent than the use of SDI alone. A more detailed study needs to be carried out to better estimate the expected performance of the SCC on the planet detection. Another important step is to set up a laboratory demonstration for the SCC. This has already started and is described in Mas et al. 2010 [20].

REFERENCES

[1] Cavarroc, C., Boccaletti, A., Baudoz, P., Fusco, T., Rouan, D., 2006, A&A, **447**, 397-403
[2] Baudoz, P., Boccaletti, A., Baudrand, J., Rouan, D., 2006, Proc. IAU Colloquium **200**, 553-558
[3] Galicher, R., Baudoz, P., 2007, C. R. Physique **8**, 333-339
[4] Galicher, R., Baudoz, P., Rousset, G., 2008, A&A, **448**, L9-L12
[5] Galicher, R., Baudoz, P., Rousset, G., Totems, J., Mas, M. 2010, A&A, **509**, A31+
[6] Baudoz, P., Rabbia, Y., Gay J., 2000, A&A**141**, 319-329
[7] Rouan, D., Riaud, P., Boccaletti, A. and Clénet, Y. and Labeyrie, A., 2000, PASP, **112**, 1479
[8] Boccaletti, A., Riaud, P., Baudoz, P., et al., 2004, PASP, **116**,1061
[9] Mawet, D. and Riaud, P. and Absil, O. and Surdej, J., 2005, ApJ, **633**, 1191
[10] Vérinaud, C., Korkiakoski, V., Yaitskova, N., Martinez, P. et al., 2008, SPIE conference, **7014**, 70141J

[11] Macintosh, B., Poyneer, L., Sivaramakrishnan, A., Marois, C., 2005, SPIE conference, **5903**, 170
[12] Marois, C., Doyon, R., Racine, R., and Nadeau, D., 2000,PASP, **112**, 91
[13] Baba, N., Murakami, N., 2003, PASP, **115**, 1363
[14] Marois, C., Lafrenière, D., Doyon, R., Macintosh, B., Nadeau, D., 2006, ApJ, **641**, 556
[15] Guyon, O. 2004, ApJ, **615**, 562
[16] Blanc, A., Fusco, T., Hartung, M., Mugnier, L., Rousset, G., 2003, A&A, **399**, 373
[17] Bordé, P., Taub, W., 2006, ApJ, **638**, 488
[18] Kasper, M, Beuzit, J.-L., Verinaud, C., Yaitskova, N. et al., 2008, SPIE conference, **7015**, 70151S
[19] Wynne, C., 1979, Opt. Comm., **28**, 21
[20] Mas, M. Baudoz, P., Rousset G., Galicher, G., Baudrand, J., Assemat, F., 2010, SPIE conference 7735